Conformation of a Spherical Polyelectrolyte Brush in the Presence of Oppositely Charged Linear Polyelectrolytes

Ran Ni, Dapeng Cao,* and Wenchuan Wang

Division of Molecular and Materials Simulation, Key Laboratory for Nanomaterials Ministry of Education, Beijing University of Chemical Technology Beijing 100029, P. R. China

Arben Jusufi†

Department of Chemical Engineering, Princeton University, Princeton, New Jersey 08544

Received April 14, 2008; Revised Manuscript Received May 14, 2008

ABSTRACT: On basis of a coarse-grained model, we investigate the conformational behavior of a spherical polyelectrolyte brush (SPB) in a solution containing oppositely charged linear polyelectrolytes. Our results obtained from Brownian dynamics (BD) simulations show that with increasing amount of linear polyelectrolytes the SPB undergoes the process of swelling → collapse → reswelling. The collapse of the SPB is due to the replacement of confined counterions by linear polyelectrolytes and is well described within a theoretical mean field approach. This replacement and a strong correlation between linear chains and SPB chains lead to a drop in the osmotic pressure inside the SPB. The reswelling is caused by further adsorption of linear chains and counterions. This in turn results in an enhanced excluded volume effect within SPB. A weak charge inversion of the SPB complex is observed. With increasing length of linear polyelectrolytes the collapse of the SPB and its reswelling is shifted toward lower concentrations of linear chains at which both effects occur. An increasing grafting density induces a multilayer structure of adsorbed linear chains and SPB chain segments. The packing process in turn increases the thickness of the SPB. We find that adsorbed linear polyelectrolytes are significantly denatured compared to the free ones in the solution.

1. Introduction

Polyelectrolyte (PE) brush is formed by densely grafted PE chains on the solid surface,[1] in which "brush" means that lengths of the polyelectrolyte chains are much larger than the average distance between the grafted sites of neighboring chains on the surface. The polyelectrolyte brushes can be generated in different geometries, such as planar,[1−6] cylindrical,[7] or spherical[8−13] PE brushes, depending on the geometry of the surface where the PE chains are densely grafted. In the past two decades the investigation on polyelectrolyte brushes has become one of the most active fields in polymer science[14,15] due to the entirely new properties of PE brushes compared with brushes of uncharged polymers and the importance in a wide range of areas, such as colloid stability,[16] rheology control,[17,18] and membrane modification.[19] In recent years, the investigation of spherical PE brushes[10] (SPB) gained a lot of scientific attention due to its widely ranged applications, such as immobilization of nanoparticles[20−23] or proteins,[15,24,25] or the grafting of DNA chains on the surface of a colloidal core particle.[26] A recent review of these investigations is given in ref 27.

The theoretical investigations on brush systems were initialized by Alexander[28] and de Gennes[29] for planar brushes assuming that the free ends of the grafted chains all lay in the same plane. On basis of the Alexander−de Gennes approach,[28,29] the theory of planar PE brush was mainly developed in the fundamental research by Pincus[16] and Borisov and co-workers.[30] A comprehensive review on the theory for planar PE brushes was addressed by Rühe et al.[1] A strong confinement of counterions inside the brush was predicted, causing a high osmotic pressure inside spherical polyelectrolyte brushes.[16] The confinement of counterions was experimentally confirmed by van der Maarel and co-workers.[31−33] Further theoretical works using scaling theory and self-consistent-field theory studied in detail the conformation of single SPBs.[34−36] The change in osmotic pressure is responsible for the interaction between SPBs.[37]

In recent years the conformational dependence on ionic strength and valency of counterions was investigated in detail for planar polyelectrolyte brushes. Theoretical mean-field approaches predicted brush shrinking and weak swelling regimes of the brush layer, depending on the valency and the concentration of the added salt.[38] A recent work predicted a collapse of planar polyelectrolyte brushes due to fluctuation effects of multivalent counterions.[39] A simulation study of rodlike PEs grafted on a plane demonstrated structural impacts due to multivalent ions.[40] The observed conformational regimes depend strongly on the grafting density. The conformational behavior of SPBs in presence of multivalent counterions has been addressed more recently by experiments, simulations, and mean-field theory. Particularly for this system, collapse transitions are of interest since they affect the overall stability of the brush suspension; coagulation effects occur in particular for collapsed SPBs.[41−43] In a most recent work the effect of multivalent ions on the SPB conformation was studied experimentally, theoretically, and with molecular dynamics simulations.[42,44] Upon addition of multivalent counterions a collapse of SPB occurs. The collapse is caused by the replacement of monovalent counterions by multivalent ones, which reduce the number of counterions inside the brush. In combination with a strong condensation of the multivalent counterions on SPB chains, the osmotic pressure inside the brush is significantly reduced.[42] A further point of interest is the interaction of SPBs with more complex ionic particles, such as proteins.[15,24,25] The question arises on the adsorption of such particles and possible denaturing phenomena of adsorbed species and the conformational properties of the SPB.

Previous investigations on the phase behavior of SPB were mainly focused on that of SPB in simple salt solutions (i.e.,

* Corresponding author: Ph 86-10-64443254; Fax 86-10-6442-7616; e-mail caodp@mail.buct.edu.cn.
† E-mail: ajusufi@princeton.edu.

10.1021/ma800827x CCC: $40.75 © 2008 American Chemical Society
Published on Web 06/11/2008

monovalent and multivalent salt) solution.[42,44] There is no simulation study regarding the structural behavior of SPB in the presence of linear polyelectrolytes of opposite charge, representing more complex "counterions". In such a system at least two effects of the mentioned ones can be studied: a collapse transition of the SPB and denaturing phenomena of adsorbed linear polyelectrolytes, i.e., the mutual impact of the SPB and the linear polyelectrolytes with respect to their corresponding configurational properties. Furthermore, we observe a reswelling of the brush upon increase of linear polyelectrolyte concentration and local charge inversion. All these effects may have an impact on the macroscopic phase behavior of SPB/polyelectrolyte solutions.

In this work we use Brownian dynamics simulation to investigate the behavior of a solution containing SPB and oppositely charged linear polyelectrolytes (LPs) on the basis of a coarse-grained implicit-solvent model. After a short description of the simulation model we focus on the collapse transition and the reswelling of the SPB by increasing the amount of oppositely charged LPs in solution. The collapse transition can be well described by a mean field theory that is briefly outlined. We then investigate the dependence of SPB conformation on the length of oppositely charged LPs and on the grafting density of the SPB. We study denaturing effects of LPs by SPB as well, which is also a problem of theoretical and practical importance.[45] We finally discuss the results with their implications on possible applications and give a brief outlook for future studies in this field.

2. Methodology

2.1. Model. We used a coarse-grained model to investigate the solution containing SPB and oppositely charged LPs. The polyelectrolyte chains are modeled as bead−spring chain consisting of Lennard-Jones (LJ) particles, as used in the polyelectrolyte models of Kremer and co-workers.[46–48] The SPB is comprised of a number of such linear polyelectrolytes end-grafted on the neutral core, and there are also a number of small ions neutralizing the solution represented by unconnected particles. The core of SPB is fixed at the center of the simulation box, and the arms in SPB are randomly end-grafted on the neutral core.[44] In contrast to a recent simulation study of rodlike PEs grafted on a plane,[40] we consider high grafting densities of flexible chains ensuring an osmotic brush behavior in the absence of LPs. In the calculations, we use N_{Arm}, f_{Arm}, and q_{Arm} denoting the length, the number of polyelectrolytes grafted on the core, and the charge of each segment in SPB arms, respectively. R_c is the radius of the SPB core. The total bare charge of a single SPB is $Q_{\mathrm{SPB}} = N_{\mathrm{Arm}} f_{\mathrm{Arm}} q_{\mathrm{Arm}}$. Similarly, the length and number of the oppositely charged LPs are M and f_{LP} with the charge of each LP segment being q_{LP}. The bare charge of a single LP is $Q_{\mathrm{LP}} = Mq_{\mathrm{LP}}$. The number of small ions and the charge of each small ion in the system are N_{I} and q_{I}, respectively. Since the small ions are added into the solution in order to neutralize the solution, their number is given by $N_{\mathrm{I}} = |(Q_{\mathrm{SPB}} + Q_{\mathrm{LP}} f_{\mathrm{LP}})/q_{\mathrm{I}}|$. All SPB and LP chain segments as well as the small ions possess the same size a.

Solvent effects are taken implicitly into account. We use Brownian dynamics simulation, in which the systems are coupled with a Langevin thermostat, and the solvent (i.e., water) enters this model through its dielectric permittivity and Brownian motion. We consider the SPB and LP chains being solvophilic, expressed by the segments interaction, as written below. While the SPB core is fixed in the center of the simulation box, the Langevin equation for the motion of each particle i holds:

$$m_i \frac{\mathrm{d}^2 \mathbf{r}_i}{\mathrm{d}t^2} = -\nabla_i U - m_i \gamma \frac{\mathrm{d}\mathbf{r}_i}{\mathrm{d}t} + \mathbf{W}_i(t) \tag{1}$$

where $m_i \equiv m$ is the particle mass which is the same for all the SPB and LP chain segments and for the small ions. U denotes the sum of all interaction potentials (see below). γ and $\mathbf{W}_i(t)$ are the friction coefficient and the stochastic force of the solvent, respectively. They are linked through the dissipation−fluctuation theorem $\langle \mathbf{W}_i(t) \cdot \mathbf{W}_j(t') \rangle = 6m\gamma k_{\mathrm{B}} T \delta_{ij} \delta(t - t')$, with $k_{\mathrm{B}}T$ being the thermal energy.

Electrostatic interaction between two charged particles with charges q_i and q_j is determined by the Coulomb potential

$$U(r_{ij}) = k_{\mathrm{B}} T l_{\mathrm{B}} \frac{q_i q_j}{r_{ij}} \tag{2}$$

where r_{ij} is the center-to-center distance between charged species. The Bjerrum length is defined as $l_{\mathrm{B}} = e^2/4\pi\epsilon_0\epsilon_{\mathrm{r}} k_{\mathrm{B}} T$, where ϵ_0 and ϵ_{r} are the permittivity of a vacuum and the relative permittivity of the solvent, respectively; e is the elementary charge.

In addition to the electrostatic interaction, for good solvent conditions, a truncated-shifted Lennard-Jones (LJ) potential is used to describe the purely repulsive excluded volume interaction between all particles except the core of SPB.

$$U_0(r_{ij}) = \begin{cases} 4\varepsilon\left[\left(\frac{a}{r_{ij}}\right)^{12} - \left(\frac{a}{r_{ij}}\right)^{6} + \frac{1}{4}\right] & \text{for } r \le 2^{1/6}a \\ 0 & \text{for } r > 2^{1/6}a \end{cases} \tag{3}$$

Here a and ε are the LJ length and energy scales, respectively. The interaction between those particles, i, and the SPB core is

$$U_0^C(r_i) = \begin{cases} \infty & \text{for } r_i \le R_c \\ U_0(r_i - R_c) & \text{for } r_i > R_c \end{cases} \tag{4}$$

The connectivity of beads into a chain (i.e., the beads in SPB arms and LPs) is maintained by the finite extensible nonlinear elastic (FENE) potential developed by Kremer and co-workers.[46–48]

$$U_{\mathrm{FENE}}(r_{ij}) = \begin{cases} -\frac{1}{2}k_0\left(\frac{R_0}{a}\right)^2 \ln\left(1 - \frac{r_{ij}^2}{R_0^2}\right) & \text{for } r_{ij} \le R_0 \\ \infty & \text{for } r_{ij} > R_0 \end{cases} \tag{5}$$

where k_0 denotes the spring constant and R_0 the maximal relative displacement between two neighboring beads. The position of the innermost segments are fixed. Those monomers experience an additional FENE type attraction, $U_{\mathrm{FENE}}^C(r_i)$, ensuring the attachment of the arms onto the core

$$U_{\mathrm{FENE}}^C(r_i) = \begin{cases} \infty & \text{for } r_i \le R_c \\ U_{\mathrm{FENE}}(r_i - R_c) & \text{for } r_i > R_c \end{cases} \tag{6}$$

2.2. Simulation Details. We performed Brownian dynamics (BD) simulations by using the open-source software LAMMPS.[49] The simulation box size is set to $L_{\mathrm{Box}} = 160a$ with periodical boundary conditions in three dimensions. The Coulomb interaction is treated with the particle−particle particle−mesh (PPPM) method.[50] The size of monomers arms is set to a = 0.25 nm.[51] In all our simulations, the reduced temperature of the system is $T^* = k_{\mathrm{B}}T/\varepsilon = 1.2$, and the Bjerrum length is l_{B} = 0.71 nm, corresponding to a value of water at room temperature. Other parameters for our simulations are $k_0 = 7.0\varepsilon$, $R_0 = 2a$, $q_{\mathrm{LP}} = -q_{\mathrm{Arm}} = 1.0$, and $\gamma = 1/\tau$, where $\tau = a(m/\varepsilon)^{1/2}$ is the LJ time unit. The counterions are monovalent as well, i.e., $q_{\mathrm{I}} = \pm 1.0$. The number of oppositely charged LPs is governed by the charge ratio, $\beta = |Q_{\mathrm{LP}} f_{\mathrm{LP}}/Q_{\mathrm{SPB}}|$, relating the total charge of LPs and that of the SPB. Counterions always ensure charge neutrality in the system. The size of the SPB core is set to R_c

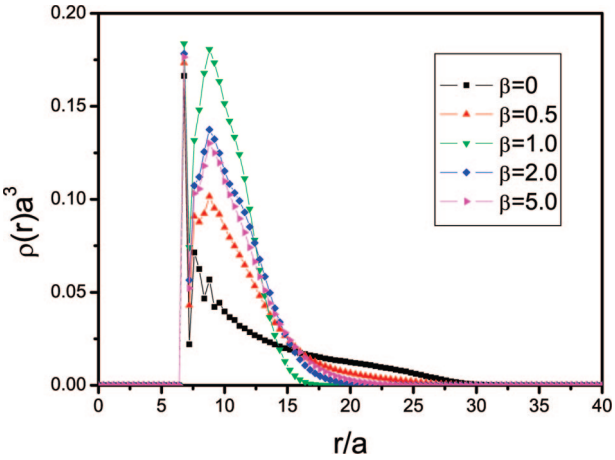

Figure 1. Density profile of brush segments with respect to the separation of the SPB center. Here the length of the brush arm is $N_{Arm} = 30$; the number of arm is $f_{Arm} = 40$. The length of linear polyelectrolytes is set to $M = 30$.

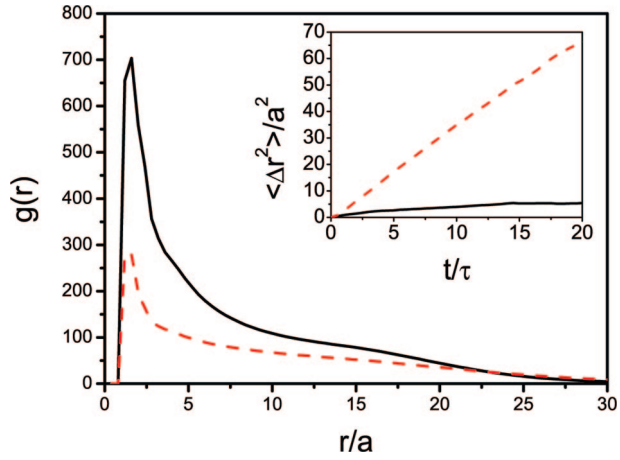

Figure 2. RDFs between arm segments and segments of linear polyelectrolytes (solid line). Shown is also the RDF between SPB monomers and counterions (dashed line). The charge ratio is $\beta = 0.5$. Inset: MSD $\langle \Delta r^2 \rangle$ of counterions (dashed line) and LP monomers (solid line) as a function of reduced time at charge ratio $\beta = 0.5$.

$= 6a$, and the length of the SPB arms is set to $N_{Arm} = 30$. Although the modeled SPB in our simulations is much smaller than the real ones in experiments, it captures the essential structural effects of the system as was demonstrated by Mei et al.[42,44]

All simulations started from randomly generated initial configurations. The simulations are performed with 400 000 simulation steps with the time step of $\Delta t = 0.005\tau$ for equilibration and following 500 000 simulation steps for production. The corresponding value of 2500τ exceeds the relaxation time of around 20τ, in agreement with findings in a recent simulation study of SPBs.[44]

3. Results and Discussion

3.1. The Brush Collapse. At first, we consider the system at various amount of LPs. The LP length was fixed at $M = 30$, and the number of LPs varies with the charge ratio β. The number of SPB chains is set to $f_{Arm} = 40$, corresponding to a grafting density $\sigma a^2 = 0.0884$. The density profiles of SPB segments, $\rho(r)$, from the SPB center with β from 0 to 5.0 are shown in Figure 1. Above $r \approx 8a$, $\rho(r)$ gradually decreases with the distance from the SPB center if no oppositely charged LPs are added, i.e., at $\beta = 0$. With increasing amount of LPs, the second peak moves from $r \approx 8a$ to $r \approx 9a$. The peak grows with the increase of β from 0 to 1. Simultaneously, the tail of the profile becomes shorter; i.e., the existence of oppositely charged LPs leads to a shrinking of the brush. Above $\beta > 1$ the first peak height of $\rho(r)$ drops again due to a reswelling of the brush; this will be discussed further below.

In order to elucidate the physical explanation for the SPB shrinking, we plot the radial distribution functions (RDFs) between the segments of the SPB arms and the LP segments, i.e. $g_{Arm\text{-}LP}(r)$, and the small SPB counterions, i.e. $g_{Arm\text{-}C}(r)$, in Figure 2 at $\beta = 0.5$, which means that the amount of LP segments equals that of the small counterions in the system. As shown in Figure 2, the correlation of the brush chains and the LP monomers is apparently stronger than that of the brush chains and the counterions. The strong correlation between SPB arms and LPs also affects the mobility of the LPs. In the inset of Figure 2 the mean-square displacement (MSD) of the LP monomers and the counterions is plotted. It proves that the mobility of the LP monomers is much smaller than that of the counterions. Compared to them, the LPs seem to be "frozen" inside the SPB. This is in line with the behavior of tri- or higher-valent counterions. We assume that in the range of $0 \le \beta \le 1$ the system behaves very analogous to the SPB in a mixture of mono- and multivalent counterions.[42,44] In what follows we present the main features of the mean-field model describing the collapse of the SPB.

Assuming that the SPB is completely neutralized by its counterions, we can neglect the osmotic pressure contributions from counterions outside of the brush. This is justified as long as the SPB is highly charged. Experimental studies has proven that more than 95% of the counterions are located inside the highly charged brush.[52] We use the concept based on the arguments of Alexander and de Gennes and extended on brush systems by Pincus and Borisov et al.[16,28–30] The chain forces consist of an elastic part and an excluded volume Flory-type contribution:

$$F_{ch} = -\frac{3k_B T f_{Arm} L}{N_{Arm} a^2} + v_0 k_B T (f_{Arm} N_{Arm})^2 \frac{9(R_c + L)^2}{8\pi[(R_c + L)^3 - R_c^3]^2} \quad (7)$$

with the excluded volume parameter $v_0 \approx a^3$ and L being the brush thickness. In equilibrium this force is balanced by the osmotic pressure forces from the confined noncondensed counterions. As discussed above, the LPs can be considered as osmotically inactive due to their strong binding on the SPB chains, as was discussed in detail in ref 44. The osmotic pressure force accounts therefore for the counterion contribution only

$$F_p^i = k_B T \xi c_+ 4\pi (R_c + L)^2 \quad (8)$$

with c_+ being the number density of SPB counterions inside the brush. However, a part of them is also osmotically inactive; i.e., they are strongly condensed. In order to account for this fraction, we introduce the parameter ξ, defined in the range $0 \le \xi \le 1$. Minimizing eqs 7 and 8 yields the brush thickness L. The parameter ξ is found for the case $\beta = 0$, i.e., without added LP. In simulations we compute $L = [\langle (R_{ce} - R_c)^2 \rangle]^{1/2}$, where R_{ce} is the center-to-end distance of the terminal monomers located at $\mathbf{r}_i^t$, which is given by $R_{ce}^2 = (1/f_{Arm}) \sum_{i=1}^{f_{Arm}} (\mathbf{r}_i^t - \mathbf{R}_c)^2$; $\mathbf{R}_c$ is the position vector of the SPB core. A reasonable match of the simulation results at $\beta = 0$, and the one computed with the mean-field theory is achieved by using $\xi = 0.6$ as used in previous studies.[42,44] This amount includes also counterions that are localized around the chains but are free to move along the chains. Only a small fraction is strictly condensed at certain SPB beads and are osmotically deactivated. We used the value $\xi = 0.6$ for all other ratios β.

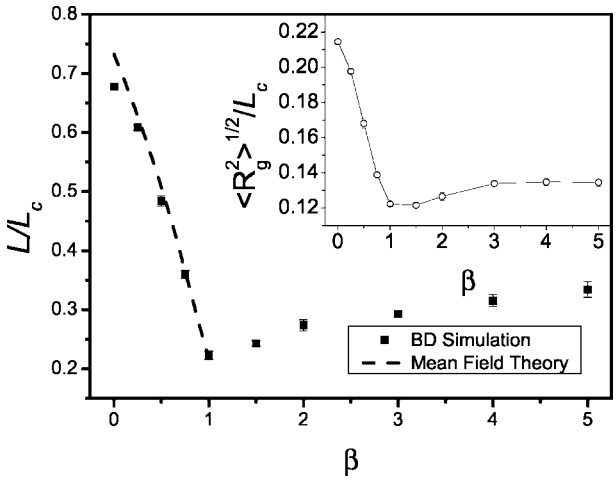

Figure 3. Relative thickness of SPB and the relative radius of gyration of SPB arms (inset) as functions of charge ratio β between LPs and SPB. The symbols are results obtained from Brownian dynamics simulation, and the dashed line represents results from mean field calculations. The solid line in the inset serves as a guide for the eye.

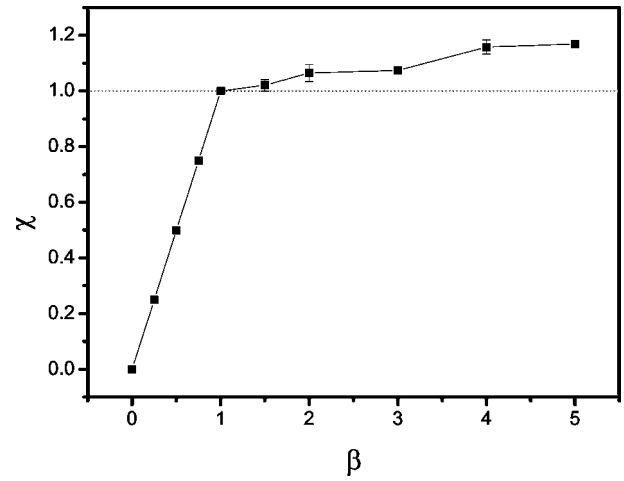

Figure 4. Charge ratio between adsorbed LPs and SPB, χ, as a function of the overall charge ratio β. Neutralization of the brush is achieved at $\chi = 1$ (dotted line).

A comparison between theory and simulation results regarding the brush thickness L is presented in Figure 3 for $\beta \leq 1$. Here, the relative thickness L/L_c, with $L_c = N_{Arm}a$ being the contour length of the SPB chains, is plotted as a function of the charge ratio β. Both results agree very well up to $\beta = 1$, the point of complete neutralization of the SPB by LPs. The collapse of SPB in solution along with the increasing amount of oppositely charged LPs is due to a reduced number of confined small counterions by LPs in conjunction with a strong condensation of LPs on SPB chains. Both effects reduce the osmotic pressure and cause the collapse of SPB. The agreement is remarkable in view of no further adjustment of the theoretical model. We treated the LPs like multivalent counterions and used exactly the same parameter setting, as in refs 42 and 44 for the case of multivalent counterions. It proves again the entropic nature of the collapse. Correlation or fluctuation effects in electrostatic contributions are of minor relevance in this range, although one could expect that those effects or other more complicated bridging effects were important for adsorbed LPs.

3.2. The Brush Reswelling Process. The mean field theory describes very well the collapse of the brush for $\beta \leq 1$. It fails, however, to account for a reswelling of the brush on further addition of LPs at $\beta > 1$. The relative brush thickness gradually increases again. Similarly, the relative radius of gyration of the individual SPB chains, $\langle R_g^2\rangle^{1/2}/L_c$, decreases and reaches a minimum at $\beta = 1.0$ and grows above this ratio. The reswelling behavior is expressed by a drop of the second peak height in $\rho(r)$ (see Figure 1). Above $\beta > 1$ the solution contains excess LPs due to strong correlation between LPs and SPB. Although the brush is completely neutralized by adsorbed LPs at $\beta \geq 1$, local correlation effects attract more LPs. For neutralization purposes, LP counterions are adsorbed as well. The excluded volume effects of the adsorbed chains and ions cause a reswelling of the brush.

We quantify the amount of adsorbed LPs with the local charge ratio between adsorbed LPs and the SPB as $\chi = |f_{Ads}Q_{LP}/Q_{SPB}|$, where f_{Ads} is the number of adsorbed LPs. They are considered as being adsorbed, if the distance between their center of masses and the SPB center is less than $R_c + L$. In Figure 4, the local charge ratio χ is plotted as a function of the overall charge ratio β. Below $\beta < 1$, all LPs in solution are adsorbed onto SPB, expressed in a strict linear behavior of $\chi(\beta)$. On further addition of LPs ($\beta > 1$) a crossover is observed. Since the charge of adsorbed LPs exceeds the bare charge of the brush, i.e., $\chi > 1$, counterions are adsorbed as well, expressed in growing peaks in their density profiles on addition of LPs β (see Figure 5a).

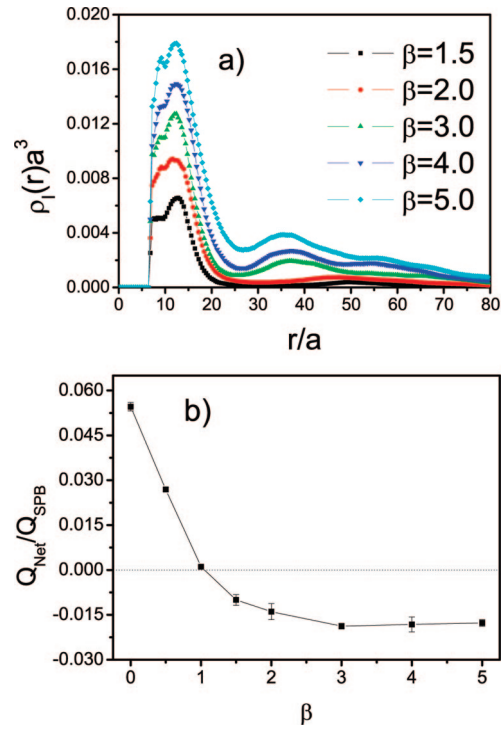

Figure 5. (a) Density profiles of small counterions as functions of the distance to the center of SPB at $\beta > 1$. (b) Relative net charge of the SPB-LP complex as a function of β. The line is a guide for the eye.

The SPB−LP complex possess a net charge Q_{Net}. For its calculation we accounted for all charges which are located inside the brush radius, $r \leq R_c + L$. We plot the relative net charge of the SPB−LP complex with respect to the bare charge Q_{SPB} in Figure 5b as a function of β. A small net charge is observed over the whole range of β. However, it is evident that a clear charge inversion takes place with a crossover at the expected value $\beta = 1$. Above $\beta > 3.0$, the net charge of the SPB−LP complex is maintained due to a saturation of adsorbed LPs. The excluded volume effect of adsorbed chains and LP counterions, in turn, increases the brush thickness, compared to the collapsed state (see Figure 3). But the brush still remains small compared to the LP free case ($\beta = 0$). In experimental studies of SPBs in

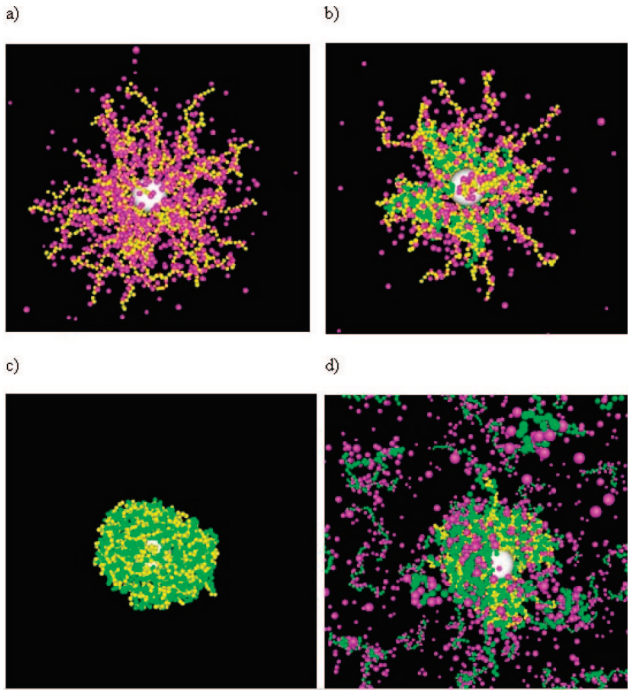

Figure 6. Simulation snapshots at different β: (a) $\beta = 0$, (b) $\beta = 0.5$, (c) $\beta = 1.0$, and (d) $\beta = 4.0$. The white sphere is the core of SPB; the yellow spheres represent SPB monomers, the green spheres are LP monomers, and the purple spheres are small counterions.

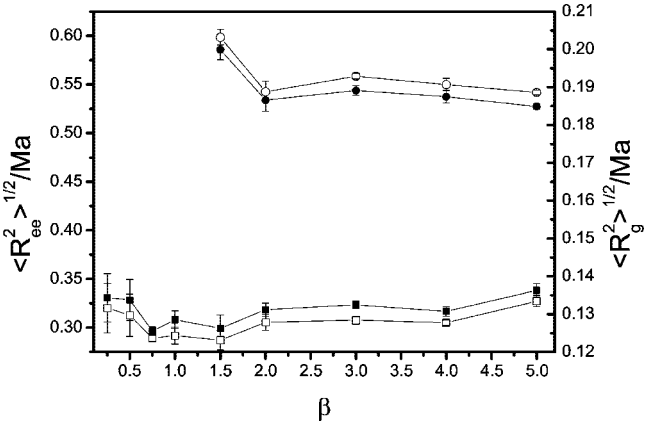

Figure 7. Relative radius of gyration (open symbols) and end-to-end distance (filled symbols) of free (circles) and adsorbed (squares) LPs as functions of charge ratio β. Lines are guides for the eye.

multivalent solution, the reswelling was not observed, and at high ionic strength SPBs coagulate.[42] Note that the ionic strength was kept constant in these works, while here the ionic strength is changed with varying β.

The snapshots of the simulated systems at different β are shown in Figure 6, and we can clearly see the collapse transition of the SPB with β increasing from 0 to 1.0, i.e. Figure 4a−c. From Figure 6d differences in the conformation of free LPs can be observed, compared to the adsorbed ones shown in Figure 6b,c. In order to quantify this conformational change, we plot in Figure 7 the relative radius of gyration and the relative end-to-end distance of adsorbed and free LPs. There are no free LPs in the solution as long as $\beta \leq 1$. Beyond that ratio, there exist some free LPs in solution. Their relative radius of gyration and end-to-end distance are around 0.195 and 0.55, respectively, whereas the values of the adsorbed LPs are around 0.125 and 0.325, respectively. These values hardly change with β. Therefore, we conclude that adsorbed LPs are significantly

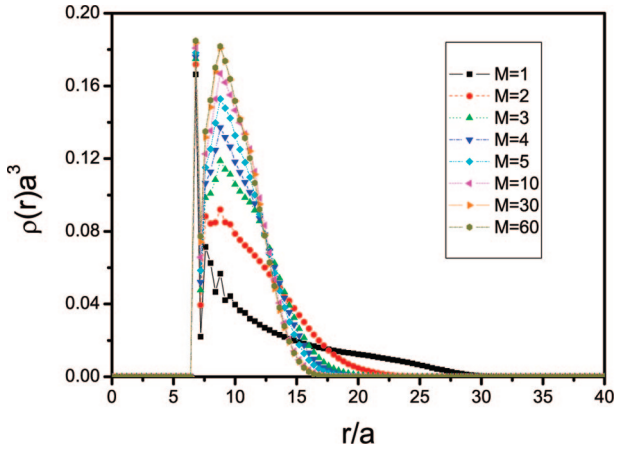

Figure 8. Density profile of brush segments from the center of the SPB core at various LP chain lengths. The length of the brush arms is $N_{Arm} = 30$, and their number is $f_{Arm} = 40$. The charge ratio between the LPs and SPB is fixed at $\beta = 1$.

denatured whereas the remaining free LPs are not affected by the presence of the SPB−LP complex.

3.3. Influence of Linear Polyelectrolyte Length and the SPB Grafting Density. In the last section we found that the SPB thickness reaches its minimum at $\beta = 1$. In this section, we investigate the influence of several factors, such as the LP length and the grafting density on the conformation of SPB.

3.3.1. Linear Polyelectrolyte Chain Length Dependence. We performed BD simulations at $\beta = 1$ with the LP length varied from 1 to 60 monomers. We kept the number of SPB arms at 40 and their degree of polymerization at 30. The density profiles of SPB monomers as functions of the distance to the center of SPB core are shown in Figure 8. For single monomers, i.e. $M = 1$, the second peak at $r \approx 8a$ is small. Its height grows and is shifted to higher distances from the SPB center (to $r \approx 9a$) when the LP length is increased. At the same time the tail of the profile shrinks. For $M \geq 3$ the brush is collapsed. However, the second peak height still evolves due to packing effects of condensed LPs, depending on their chain length. Above $M > 10$, the density profiles of SPB arms hardly change. The mentioned packing effects are reflected in the correlations between LPs and SPB arms segments (see their RDFs in Figure 9a). The first correlation peak increases with the chain length M. At $M = 1$, the height of the contact peak of $g_{Arm\text{-}LP}(r)$ is around 290. This peak grows significantly with increasing LP chain length. In addition, a second peak appears for longer chains ($M > 5$). The strong SPB−LP correlation, in turn, affects the mobility of the LPs as well, as expressed by their MSD (see Figure 9b). The slope of MSD vs time sharply decreases with the LP length, resulting in a reduced mobility.

The strong condensation of LPs is again the main reason for the collapse of the brush at this charge ratio ($\beta = 1$). This is in analogy with the conformation of SPB in solution containing multivalent salt with increasing valence of the salt ions.[42,44] The relative thickness of SPB and the relative gyration radius of SPB arms as functions of the LP length are plotted in Figure 10. In accordance with the above observations of the density profiles, the SPB collapses with increased LP length. Up to $M < 3$ the SPB shrinks dramatically from 0.68 to 0.3 in terms of its relative thickness L/L_c. This is in line with the study of SPBs in presence of multivalent counterions.[44] However, the brush continues its shrinking above $M > 3$ until it saturates at around 0.23 for $M > 5$. This further brush thickness reduction has not been reported for SPBs in the presence of multivalent counterions. There, the saturation is already reached for trivalent counterions. Obviously, the chainlike characteristic of adsorbed LPs causes a further slight shrinking.

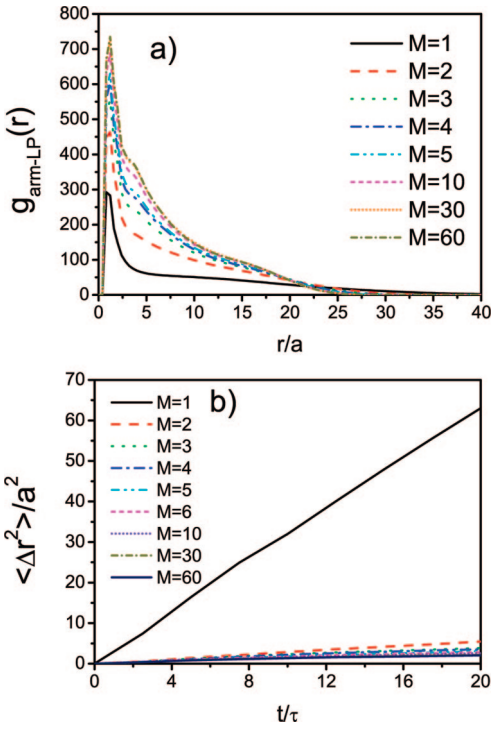

Figure 9. (a) RDFs between segments of SPB arms and LP chains. (b) MSD $\langle \Delta r^2 \rangle$ of LP monomers vs time. The charge ratio is set to $\beta = 1$.

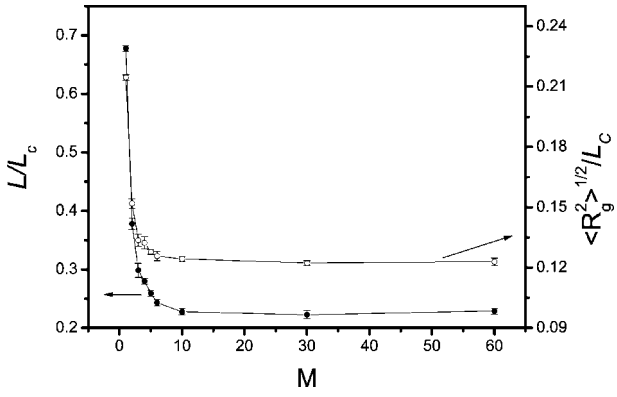

Figure 10. Relative thickness of the SPB (filled symbols) and the relative radius of gyration of SPB arms (open symbols) as functions of the length of linear polyelectrolytes at $\beta = 1$.

We now vary the charge ratio β. For the previous case, $M = 30$, we observed a continuous reswelling of SPB for $\beta > 1$ (see Figure 3). The relative SPB thickness and radius of gyration of SPB arms for LPs with length $M = 2$, 5, and 30 are shown in Figure 11. Again the SPB collapse is completed at $\beta = 1$, reaching a minimum. However, the minimum values are different, as discussed above. The result for $M = 2$ is in line with previous simulations of SPBs in the presence of divalent ions.[44] The dashed line shown in Figure 11 is the mean field result for $M = 2$, assuming that, in addition to the monovalent counterions, around 1/3 of LPs contribute to the osmotic pressure as well. This value is the same as used for divalent counterions; see ref 44 for further details. The solid line is the mean field result for $M = 5$ and $M = 30$; i.e., no LPs contribute to the osmotic pressure inside the brush. The mean field theory predicts the collapse very well. Again, the drop in the osmotic pressure is the driving force for the collapse. The reswelling effect, however, cannot been captured within the theoretical approach. In conclusion, it is shown that the increase of the LP length dramatically strengthens the correlation between SPB and LPs,

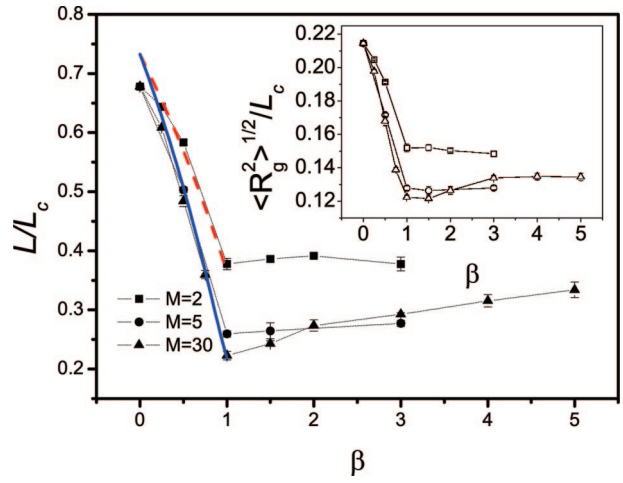

Figure 11. Relative thickness of SPB (filled symbols) and the relative radius of gyration of SPB arms (open symbols) as functions of charge ratio between LPs and SPB at several chain lengths of LPs. The thick solid and dashed lines are theoretical results with $M = 30$ and $M = 2$, respectively. Note that the results for $M = 5$ are the same. The thin lines are guides for the eye.

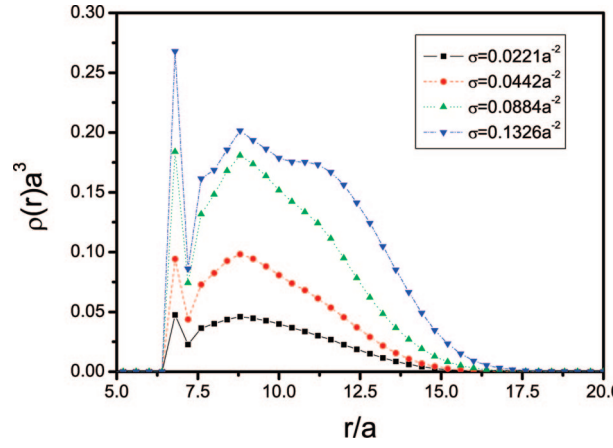

Figure 12. Density profiles of brush segments from the center of the SPB core at various grafting densities and at $\beta = 1$.

causing an amplified collapse and pronounced reswelling of the SPB.

3.3.2. Influence of the SPB Grafting Density. We now investigate the influence of grafting density on the conformation of SPB at $\beta = 1$. We performed BD simulations with grafting density of SPB at $\sigma = 0.0221a^{-2}$, $0.0442a^{-2}$, $0.0844a^{-2}$, and $0.1326a^{-2}$, corresponding to chain numbers $f_{Arm} = 10$, 20, 40, and 60 at constant degree of polymerization $N_{Arm} = 30$.

The density profiles of the SPB monomers as functions of the distance to the center of SPB are shown in Figure 12. There are two peaks of $\rho(r)$, one contact peak at $r \approx 7a$ and one at $r \approx 9a$ at small grafting densities, e.g., at $\sigma = 0.0221a^{-2}$. With denser grafting, the heights of both peaks increase. This increase becomes more gradual at higher grafting densities. At the same time, a shoulder peak located at $r = 11a$ appears as well, particularly pronounced for $\sigma = 0.1326a^{-2}$. The peaks are caused by packing arrangements of the SPB monomers around the core, in particular at higher grafting densities. The density profiles of LP monomers, $\rho_{LP}(r)$, possess a similar behavior (see Figure 13). There is only one peak located at $r = 8.0a$ for $\sigma = 0.0224a^{-2}$. Its position hardly changes with increasing grafting density. However, the peak height and the establishment of a second peak at around $r = 10a$ occur, in particular for $\sigma \geq 0.0442a^{-2}$. A strong binding of LPs on SPB chains causes packing arrangements of LP segments. This arrangements follow

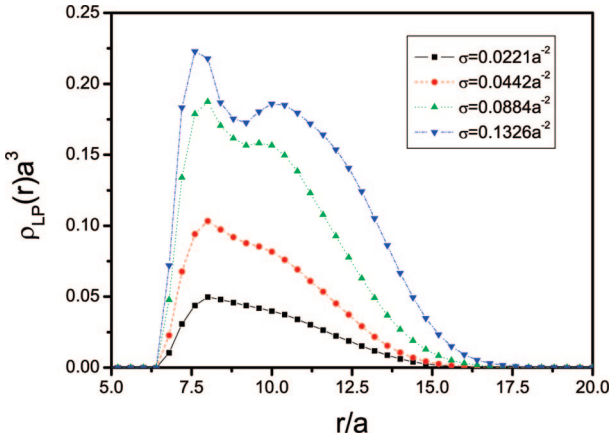

Figure 13. Density profiles of LP monomers from the center of the SPB core at various grafting densities and at $\beta = 1$.

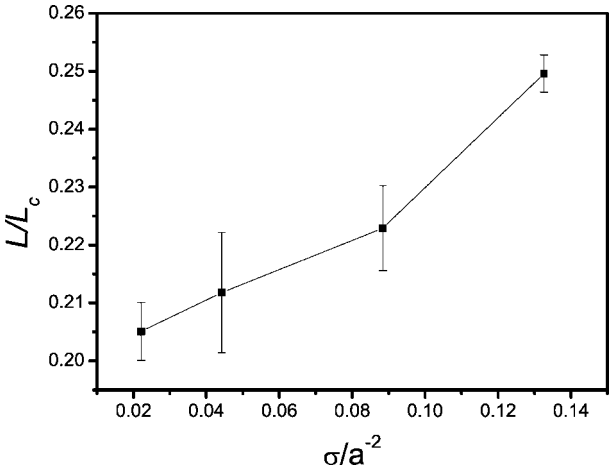

Figure 14. Relative thickness of SPB as a function of grafting density at $\beta = 1$.

a layer-by-layer process, starting with the packing close to the colloidal core surface, and continue with a subsequent filling of the second layer until the brush is neutralized. This multilayer adsorption is similar to the adsorption of polyelectrolytes on oppositely charged macroions.[53]

The influence of grafting density on the SPB thickness is shown in Figure 14. The thickness increases monotonically with the grafting density of SPB. The slope is superlinear due to establishments of subsequent layers of SPB and LP monomers. The multilayer structure is mostly pronounced for $\sigma = 0.1326a^{-2}$; see the corresponding density profiles in Figures 12 and 13.

Finally, we calculated the mean electrostatic potential (MEP) around the SPB, $\Psi(r)$,[53] via

$$\Psi(r) = \frac{e}{\epsilon_0 \epsilon_r} \int_r^\infty [\rho(r')q_{\mathrm{Arm}} + \rho_{\mathrm{LP}}(r')q_{\mathrm{LP}}]\left[r' - \frac{r'^2}{r}\right] \mathrm{d}r' \quad (9)$$

The calculated $\Psi(r)$ as a function of the distance to the center of SPB is plotted in Figure 15. At small grafting density, i.e. $\sigma = 0.0221a^{-a}$, $\Psi(r)$ monotonically increases from -24 to 5.5 mV, followed by a damped oscillation that converges rapidly to zero. The oscillation stems from the multilayer structures, as discussed above. When the grafting density is increased from $\sigma = 0.0221a^{-2}$ to $0.0884a^{-2}$, the first (positive) peak depreciates. The charge inversion at this point becomes weaker. Interestingly, when the grafting density of SPB reaches $0.1326a^{-2}$, the positive peak "bounces" back to 5.5 mV; i.e., charge inversions inside the SPB are not monotonic functions of the grafting density.

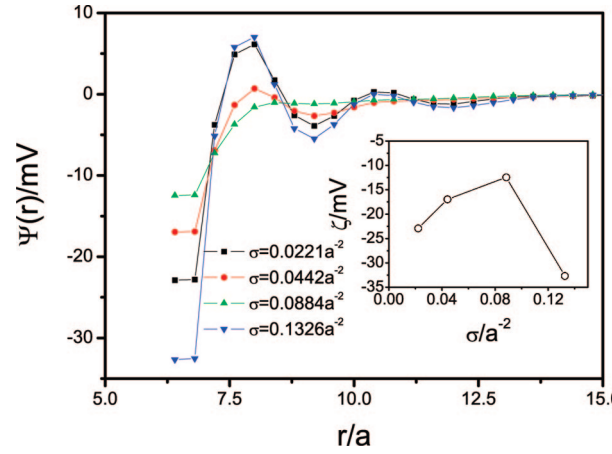

Figure 15. Mean electrostatic potential around the SPB as a function of the distance from the SPB center at $\beta = 1$. Inset: ζ-potential as a function of the grafting density at $\beta = 1$.

The stability of electrical layer of the monomers within the SPB is directly related to the ζ -potential, which is the mean electrostatic potential at the shortest separation from the core surface. The ζ -potential is plotted as a function of the grafting density in the inset of Figure 15. Similar to the nonmonotonic behavior of the first peak in $\Psi(r)$, the ζ -potential of the electrical layer increases at first and then drops again with enhanced grafting density. This is in analogy to the results of polyelectrolyte complexation on oppositely charged macroions.[53]

4. Conclusions

On the basis of a coarse-grained model, we investigated the conformational behavior of a spherical polyelectrolyte brush (SPB) in the presence of a mixture of monovalent counterions and oppositely charged linear polyelectrolytes (LPs). We specifically studied the influence of LP on the SPB structure and varied parameters such as grafting density and the length of LP chains. Vice versa, we also investigated the denaturing effects of adsorbed LPs in comparison to free LPs. Adsorbed LP chains are much less extended than the free ones; i.e., adsorption is accompanied by denaturation of the LPs.

Our simulation results showed that with increasing amount of LPs the SPB collapses in a charge ratio range $0 \leq \beta \leq 1$. From our structural analysis we found that the SPB counterions are completely replaced by LP chains. On average, each adsorbed LP chain of length M replaces M counterions, which reduces the osmotic pressure inside the brush. A strong binding of LPs on SPB chains was observed, leading to a reduced mobility of the adsorbed chains. The LP−SPB correlation amplifies the drop in the osmotic pressure, which leads to a full collapse at $\beta = 1$, i.e., when the brush is completely neutralized by LP chains. Moreover, we also employed a mean field theory to describe the collapse transition of SPB from $\beta = 0$ to 1. The theoretical model has been shown to be well suited to describe the collapse of SPBs in presence of a mixture of mono- and multivalent counterions.[42,44] We applied the same model with the same parameters also for the present system. The mean field results could describe the collapse very well. It strengthens the previous argument that the collapse is mainly of entropic nature. On further addition of LP chains ($\beta > 1$) a reswelling was observed, which cannot be captured by the mean field theory. A charge inversion occurs for $\beta > 1$. The relative net charge is small, but in view of a high bare charge of real SPBs (around 10^5−10^6 charges)[27] the absolute charge number can be significant and can have important implications for static and kinetic behavior of SPB−LP solutions. The reswelling of SPB in multivalent salt solution has not been observed so far.

We believe that this is caused by strong attractive correlation effects between SPB and LPs. Excluded volume effects of adsorbed LPs and their counterions leads to this reswelling.

The collapse and reswelling effect depend on the chain length of LPs. Short chains ($M \leq 5$) possess different degrees of collapsed states at $\beta = 1$; i.e., up to $M = 5$ the minimum of the brush thickness depreciates, and no pronounced reswelling on further addition of LP occurs. This is not the case of SPBs in presence of multivalent ions. There the saturation is already reached for trivalent counterions at around 30% of the contour length.[44] For chainlike "counterions", longer chains ($M > 5$) cause a slightly lower saturation level, at around 23% of the contour length.

The grafting density of SPB chains influences the conformational behavior as well. With increased grafting density the SPB and LP chains undergo packing process, which forms a multilayer structure around the SPB core. The thickness of the collapsed SPB is monotonically augmented by the increased grafting density as well. We also calculated the mean electrostatic potential of the electrical layer around the core of SPB. The results demonstrate that local charge inversion occurs due to the mentioned multilayer structures of the chains inside the brush. The concomitant ζ-potential possess a nonmonotonic behavior with regard to the grafting density.

It would be interesting to observe the impact of the studied effects on the phase behavior of SPBs, such as the occurrence of coagulation effects, as they appear for SPBs in even simple salt solutions.[42,43] It is assumed that coagulation is mainly driven due to short-ranged dispersion forces of the core particle. Those forces are not balanced if the brush is collapsed. However, further addition of LPs could stabilize a SPB dispersion again due to reswelling and charge inversion of the SPB−LP complex. This is similar to salting-in and salting-out effects as observed experimentally for SPBs in the presence of simple salt ions at high ionic strengths.[43] However, in the present case those effects can occur at minute LP concentrations. And it is not clear yet whether attractive forces due to bridging effects—caused by multivalent ions or LPs—could enhance coagulation processes. For the study of those macroscopic effects simulations of two or more SPBs would be necessary with a focus on possible attractive correlation forces between SPBs.

Acknowledgment. R.N. thanks Prof. Andrey V. Dobrynin and Jan-Michael Y. Carrill in University of Connecticut and Paul Crozier in Sandia National Laboratories for their help on using LAMMPS. This work is supported by National Natural Science Foundation of China (No. 20776005, 20736002), the Beijing Novel Program (2006B17), NCET from Ministry of Education (NCET-06-0095), the "Chemical Grid Program", and the Excellent Talent Foundation from BUCT. A.J. gratefully acknowledges financial support by the Deutsche Forschungsgemeinschaft (DFG).

References and Notes

(1) Rühe, J.; Ballauff, M.; Biesalski, M.; Dziezok, P.; Grohn, F.; Johannsmann, D.; Houbenov, N.; Hugenberg, N.; Konradi, R.; Minko, S.; et al. *Adv. Polym. Sci.* **2004**, *165*, 79.
(2) Ahrens, H.; Förster, S.; Helm, C. A. *Macromolecules* **1997**, *30*, 8447.
(3) Biesalski, M.; Rühe, J. *Macromolecules* **1999**, *32*, 2309.
(4) Currie, E. P. K.; Sieval, A. B.; Avena, M.; Zuihof, H.; Sudholter, E. J. R.; Cohen, S. M. A. *Langmuir* **1999**, *15*, 7116.
(5) Tamashiro, M. N.; Hernández-Zapata, E.; Schorr, P. A.; Balastre, M.; Tirrell, M. *J. Chem. Phys.* **2001**, *115*, 1960.
(6) Bendejacq, D.; Ponsinet, V.; Joannicot, M. *Eur. Phys. J. E* **2004**, *13*, 3.
(7) Muller, F.; Delsanti, M.; Auvray, L.; Yang, J.; Chen, Y. J.; Mays, J. W.; Deme, B.; Tirrell, M.; Guenoun, P. *Eur. Phys. J. E* **2000**, *3*, 45.
(8) Zhang, L.; Yu, K.; Eisenberg, A. *Science* **1996**, *272*, 1777.
(9) Biver, C.; Hariharan, R.; Mays, J. W.; Russel, W. B. *Macromolecules* **1997**, *30*, 1787.
(10) Guo, X.; Weiss, A.; Ballauff, M. *Macromolecules* **1999**, *32*, 6043.
(11) Muller, F.; Fontaine, P.; Delsanti, M.; Belloni, L.; Yang, J.; Chen, Y. J.; Mays, J. W.; Lesieur, P.; Tirrell, M.; Guenoun, P. *Eur. Phys. J. E* **2001**, *6*, 109.
(12) Lee, A.; Butun, V.; Vamvakaki, M.; Armes, S. P.; Pople, J. A.; Gast, A. P. *Macromolecules* **2002**, *35*, 8540.
(13) Förster, S.; Hermsdorf, N.; Bottcher, C.; Lindner, P. *Macromolecules* **2002**, *35*, 4096.
(14) Zhou, F.; Huck, W. T. S. *Phys. Chem. Chem. Phys.* **2006**, *8*, 3815.
(15) Wittemann, A.; Ballauff, M. *Phys. Chem. Chem. Phys.* **2006**, *8*, 5269.
(16) Pincus, P. *Macromolecules* **1991**, *24*, 2912.
(17) Amoskov, M.; Birshtein, T. M.; Belyaev, D. K. *J. Polym. Sci., Ser. A* **2007**, *49*, 851.
(18) Marra, A.; Peuvrel-Disdier, E.; Wittemann, A.; Guo, X.; Ballauff, M. *Colloid Polym. Sci.* **2003**, *281*, 491.
(19) Jain, P.; Dai, J.; Grajales, S.; Saha, S.; Baker, G. L.; Bruening, M. L. *Langmuir* **2007**, *23*, 11360.
(20) Sharma, G.; Ballauff, M. *Macromol. Chem., Rapid Commun.* **2004**, *25*, 547.
(21) Sharma, G.; Mei, Y.; Ballauff, M.; Irrgang, T.; Kempe, R. *J. Catal.* **2007**, *246*, 10.
(22) Mei, Y.; Lu, Y.; Polzer, F.; Ballauff, M.; Drechsler, M. *Chem. Mater.* **2007**, *19*, 1062.
(23) Mei, Y.; Sharma, G.; Lu, Y.; Ballauff, M. *Langmuir* **2005**, *21*, 12229.
(24) Wittemann, A.; Haupt, B.; Ballauff, M. *Phys. Chem. Chem. Phys.* **2003**, *5*, 1671.
(25) Rosenfeldt, S.; Wittemann, A.; Ballauff, M.; Breininger, E.; Bolze, J.; Dingenouts, N. *Phys. Rev. E* **2004**, *70*, 061403.
(26) Kegler, K.; Salomo, M.; Kremer, F. *Phys. Rev. Lett.* **2007**, *98*, 058304.
(27) Ballauff, M. *Prog. Polym. Sci.* **2007**, *32*, 1135.
(28) Alexander, S. *J. Phys. (Paris)* **1977**, *38*, 983.
(29) de Gennes, P. G. *Macromolecules* **1980**, *13*, 1069.
(30) Borisov, O. V.; Birshtein, T. M.; Zhulina, E. B. *J. Phys. II* **1991**, *1*, 521.
(31) van der Maarel, J. R. C.; Groenewegen, W.; Egelhaaf, S. U.; Lapp, A. *Langmuir* **2000**, *16*, 7510.
(32) Groenewegen, W.; Lapp, A.; Egelhaaf, S. U.; van der Maarel, J. R. C. *Macromolecules* **2000**, *33*, 8152.
(33) Groenewegen, W.; Egelhaaf, S. U.; Lapp, A.; van der Maarel, J. R. C. *Macromolecules* **2000**, *33*, 3283.
(34) Borisov, O. V.; Zhulina, E. B. *J. Phys. II* **1997**, *7*, 449.
(35) Borisov, O. V.; Zhulina, E. B. *Eur. Phys. J. B* **1998**, *4*, 205.
(36) Klein-Wolterink, J.; Leermakers, F. A. M.; Fleer, G. J.; Koopal, L. K.; Zhulina, E. B.; Borisov, O. V. *Macromolecules* **1999**, *32*, 2365.
(37) Jusufi, A.; Likos, C. N.; Ballauff, M. *Colloid Polym. Sci.* **2004**, *282*, 910.
(38) Zhulina, E. B.; Borisov, O. V.; Birshtein, T. M. *Macromolecules* **1999**, *32*, 8189.
(39) Santangelo, C. D.; Lau, A. W. C. *Eur. Phys. J. E* **2004**, *13*, 335.
(40) Fazli, H.; Golestanian, R.; Hansen, P. L.; Kolahchi, M. R. *Europhys. Lett.* **2006**, *73*, 429.
(41) Guo, X.; Ballauff, M. *Phys. Rev. E* **2001**, *64*, 051406.
(42) Mei, Y.; Lauterbach, K.; Hoffmann, M.; Borisov, O. V.; Ballauff, M.; Jusufi, A. *Phys. Rev. Lett.* **2006**, *97*, 158301.
(43) Mei, Y.; Ballauff, M. *Eur. Phys. J. E* **2005**, *16*, 341.
(44) Mei, Y.; Hoffmann, M.; Ballauff, M.; Jusufi, A. *Phys. Rev. E* **2008**, *77*, 031805.
(45) Hsiao, P.-Y.; Luijten, E. *Phys. Rev. Lett.* **2006**, *97*, 148301.
(46) Grest, G. S. *Macromolecules* **1994**, *27*, 3493.
(47) Stevens, M. J.; Kremer, K. *J. Chem. Phys.* **1995**, *103*, 1669.
(48) Grest, G. S.; Kremer, K.; Witten, T. A. *Macromolecules* **1987**, *20*, 1376.
(49) Plimpton, S. J. *J. Comput. Phys.* **1995**, *117*, 1.
(50) Frenkel, D.; Smit, B. *Understanding Molecular Simulation—From Algorithm to Applications*; Academic Press: New York, 1996.
(51) Romet-Lemonne, G.; Daillant, J.; Guenoun, P.; Yang, J.; Mays, J. W. *Phys. Rev. Lett.* **2004**, *93*, 148301.
(52) Das, B.; Guo, X.; Ballauff, M. *Prog. Colloid Polym. Sci.* **2003**, *121*, 34.
(53) Ni, R.; Cao, D. P.; Wang, W. C. *J. Phys. Chem. B* **2006**, *110*, 26232.

MA800827X